THE ASTROPHYSICAL JOURNAL, 484:L75–L78, 1997 July 20


# ASSOCIATION OF EXTREME-ULTRAVIOLET IMAGING TELESCOPE (EIT) POLAR PLUMES WITH MIXED-POLARITY MAGNETIC NETWORK

Y.-M. WANG, N. R. SHEELEY, JR., K. P. DERE, R. T. DUFFIN,[1] R. A. HOWARD, D. J. MICHELS, AND J. D. MOSES
E. O. Hulburt Center for Space Research, Naval Research Laboratory, Washington, DC 20375-5352

J. W. HARVEY AND D. D. BRANSTON
National Solar Observatory, Tucson, AZ 85726

J.-P. DELABOUDINIÈRE, G. E. ARTZNER, AND J. F. HOCHEDEZ
Institut d'Astrophysique Spatiale, F-91405 Orsay Cedex, France

J. M. DEFISE
Centre Spatial de Liège, B-4031 Angleur, Belgium

R. C. CATURA AND J. R. LEMEN
Lockheed Palo Alto Research Laboratory, Palo Alto, CA 94304

J. B. GURMAN, W. M. NEUPERT, J. NEWMARK, AND B. THOMPSON
NASA/Goddard Space Flight Center, Greenbelt, MD 20771

A. MAUCHERAT
Laboratoire d'Astronomie Spatiale, F-13376 Marseille Cedex 12, France

AND

F. CLETTE
Observatoire Royal de Belgique, B-1180 Bruxelles, Belgium
*Received 1997 April 4; accepted 1997 May 7*

## ABSTRACT

*SOHO* EIT spectroheliograms showing the polar coronal holes during the present sunspot minimum are compared with National Solar Observatory (Kitt Peak) magnetograms taken in Fe I λ8688 and Ca II λ8542. The chromospheric λ8542 magnetograms, obtained on a routine, near-daily basis since 1996 June, reveal the Sun's strong polar fields with remarkable clarity. We find that the Fe IX λ171 polar plumes occur where minority-polarity flux is in contact with flux of the dominant polarity inside each polar hole. Moreover, the locations of "plume haze" coincide approximately with the patterns of brightened He II λ304 network within the coronal hole. The observations appear to be consistent with mechanisms of plume formation involving magnetic reconnection between unipolar flux concentrations and nearby bipoles. The fact that minority-polarity fields constitute only a small fraction of the total magnetic flux within the polar holes suggests that plumes are not the main source of the high-speed polar wind.

*Subject headings:* solar wind — Sun: chromosphere — Sun: corona — Sun: magnetic fields — Sun: UV radiation — Sun: X-rays, gamma rays

## 1. INTRODUCTION

When observed in the extreme-ultraviolet (EUV), polar plumes appear as diffuse, spikelike or sheetlike structures within the polar coronal holes (see, e.g., Bohlin, Sheeley, & Tousey 1975; Ahmad & Withbroe 1977; Habbal 1992; DeForest 1995). The high density of the plume gas relative to the interplume background implies that a strong heating source is present near the base of the plume (Wang 1994; Habbal et al. 1995). In an earlier study (Wang & Sheeley 1995), an effort was made to identify this heating source using EUV images obtained during 1973–1974 with the slitless spectroheliograph on *Skylab*. It was found that the diffuse, plumelike Mg IX λ368 structures within polar and lower latitude coronal holes occurred near collections of compact Ne VII λ465 emission features, whose locations in turn coincided with relative brightenings in the He II λ304 network. Because such network enhancements are believed to be associated with magnetic bipoles (see, e.g., Harvey 1985, who studied the analogous darkenings in the He I λ10830 network), it was inferred that coronal plumes occurred in the vicinity of mixed-polarity fields. The same conclusion was suggested by comparing the locations of Mg IX "haze" inside a low-latitude coronal hole with a high-resolution magnetogram. However, direct comparisons between the *Skylab*-era polar plumes and the underlying distribution of magnetic flux could not be made because of the lack of simultaneous, high-quality magnetograms of the polar regions.

The successful launch of the *Solar and Heliospheric Observatory* (*SOHO*) at the end of 1995 has provided a new opportunity to investigate the magnetic nature of polar plumes. In this Letter, we compare images of the polar coronal holes obtained using the Extreme-ultraviolet Imaging Telescope (EIT) on *SOHO* with Fe I λ8688 and Ca II λ8542 magnetograms recorded at the National Solar Observatory (NSO) at Kitt Peak.

## 2. THE OBSERVATIONS

A detailed description of the EIT instrument is given by Delaboudinière et al. (1995). The telescope, in continuous

[1] Computational Physics, Inc.

operation since early 1996, records images of the Sun in four selected emission lines: Fe IX λ171, Fe XII λ195, Fe XV λ284, and He II λ304. The mirrors are divided into four corresponding quadrants, each with a multilayer coating tuned to the given wavelength. A rotating mask allows only a single quadrant to be illuminated at any one time, and the resulting image is focused onto a $1024 \times 1024$ pixel CCD. The aluminum filters that block out long-wavelength radiation and stray light are supported by wire meshes, which produce a faint grid pattern on the images.

For comparison with the ground-based magnetograms described below, we employ half-resolution (∼5″ pixel size) images taken in Fe IX λ171 and He II λ304 from mid-1996 onward. These full-disk spectroheliograms were made daily around 19:00 UT as part of the EIT synoptic program. Because the peak emissivity in the Fe IX λ171 line occurs at $T \simeq 1 \times 10^6$ K, which coincides with the characteristic temperature of EUV polar plumes (Bohlin et al. 1975; Widing & Feldman 1992), the λ171 images show the plumes at their brightest and most extended (although they are also well visible in the EIT Fe XII λ195 images). By contrast, the chromospheric network structure and the coronal hole boundaries are seen most clearly in the He II λ304 spectroheliograms, which can therefore be used to identify compact features around the bases of the Fe IX plumes and to verify that the plumes are indeed rooted inside the polar holes.

Since the 1970s, full-disk photospheric magnetograms and He I λ10830 spectroheliograms have been recorded on a daily basis with the NSO Vacuum Telescope on Kitt Peak (Livingston et al. 1976a). On rare occasions, images were taken in other spectral lines (including Ca II λ8542) using the original magnetograph (Livingston et al. 1976b). The installation of a much-improved magnetograph (Jones et al. 1992) allowed regular full-disk magnetograms in Ca II λ8542 to be added to the daily observing program starting 1996 June 27. These "chromospheric" magnetograms are generally made sometime between 17:00 and 21:00 UT (nicely bracketing the EIT synoptic observations), after the Fe I λ8688 magnetogram and the He I λ10830 spectroheliogram have been completed. (Each full-disk scan takes from 1 to 2 hr.) For the purposes of this study, half-resolution (2.″3 pixel size) versions of the three types of images were obtained from NSO/Kitt Peak by anonymous ftp; the maps were then rebinned to one-quarter resolution (∼5″ pixel size) by $2 \times 2$ pixel averaging. We have also scaled the λ8688 and λ8542 measurements upward by factors of 1.46 and 2.15, respectively. These correction factors take into account the Landé $g$-factor of the spectral line, the dispersion of the spectrograph, the efficiency of the polarization modulator, and a phase lag associated with the CCD camera.

## 3. COMPARISON OF MAGNETOGRAMS AND EIT IMAGES

The relationship between the observed polar fields and the EUV structures within the polar coronal holes is best seen by comparing the different images visually. The examples shown and discussed in this section have been chosen from a large body of similar data available for the 1996–1997 sunspot minimum.

Figure 1 (Plate L4) shows the north polar hole on 1996 August 15. The magnetic flux distributions measured using Fe I λ8688 and Ca II λ8542 are compared in the top two panels. Allowing for the 2 hr difference between the times of observation, we see the same general patterns of positive- and negative-polarity flux elements; positive polarity is overwhelmingly dominant in both cases. However, whereas the flux elements in λ8688 form irregular, broken fragments, in λ8542 they appear as smoother clumps. Much of this difference can undoubtedly be attributed to the rapid fanning-out of the magnetic flux tubes in the chromosphere. Thus, at the heights just below the temperature minimum where the λ8688 absorption line originates, the field will be concentrated into relatively small clumps at the supergranular cell boundaries, whereas at the greater heights where λ8542 is formed (∼1000 km above the temperature minimum), the field will have spread to cover a significant fraction of the cell interior (see Chapman & Sheeley 1968a; Giovanelli 1980; Jones 1985). At the same time, asymmetries in the horizontal field component may affect the magnitude of $B_{\rm los}$ as measured in λ8542 near the limb. There will also be a general tendency for the magnetic field within the coronal hole to become increasingly unipolar (positive-polarity in Fig. 1) with height, as more and more of the minority-polarity flux closes down and becomes "trapped" inside low-lying bipoles.

A well-known characteristic of strong canopy fields is the appearance, toward the limb, of "false" polarities associated with the horizontal field component (Chapman & Sheeley 1968b; Pope & Mosher 1975; Giovanelli 1980). However, an inspection of the magnetograms in Figures 1–6 suggests that most of the black (white) features do in fact represent radially inward (radially outward) directed fields, for two reasons: first, we see little evidence for any systematic limbward "fringing" or black-white doubling of the flux elements, and, second, in those cases where a white (black) clump in λ8542 has a black (white) clump on its limbward side, the λ8688 magnetogram (which should be less susceptible to the fringing effect) shows that both polarities are present at lower heights. Nevertheless, the effect of the horizontal canopy fields on the magnetograph signal near the poles is poorly understood and remains to be properly evaluated.

The bottom two panels of Figure 1 show the north polar hole in Fe IX λ171 and He II λ304. These EIT images were made around 20:00 UT, about 90 minutes after the same polar area was scanned in λ8688 and 20 minutes before it was scanned in λ8542. The brightest of the foreground Fe IX plumes occur where large chunks of positive- and negative-polarity flux are contiguous to each other in the λ8542 magnetogram. From a comparison of the two EIT images, we also see that the bright plumes are located above areas of strong He II network emission (although not every network bright point is accompanied by proportionately strong plume emission). Further, we note that compact, looplike Fe IX structures are sometimes visible where intense He II network is present (e.g., near the left edge of the images).

Figure 2 (Plate L5) shows the north polar hole on 1996 October 12. The difference between the magnetograms taken in λ8688 and λ8542 is again apparent: the latter shows large chunks of flux (particularly in the dominant, positive polarity) that remain clearly visible all the way to the limb, whereas the corresponding patterns in λ8688 are more noisy and fragmentary, with a greater intermixture of positive- and negative-polarity flux elements. Comparing the EIT images with the λ8542 magnetogram, we see a general correspondence between the patterns of Fe IX emission (consisting of both plumelike haze and low-lying, compact features), the areas of brightened He II network, and the regions where sizable

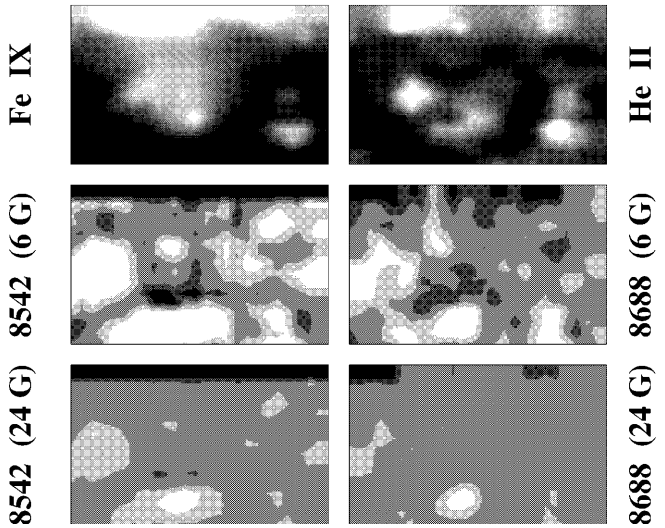


FIG. 4.—Enlargement of an area inside the north polar hole on 1996 November 8. The four panels are in approximate register, with the north polar limb located near the top of each panel. *Top left*: Fe IX λ171 spectroheliogram (19:00 UT). Note the looplike structure on the east side of the plume. *Top right:* He II λ304 spectroheliogram (19:05 UT), showing network brightenings and intense bright points. *Middle left:* chromospheric magnetogram in Ca II λ8542 (18:52–19:04 UT). *Middle right:* photospheric magnetogram in Fe I λ8688 (16:41–16:47 UT). *Bottom left:* Ca II λ8542 magnetogram (strong fields only). *Bottom right:* Fe I λ8688 magnetogram (strong fields only). In the two middle panels, gray-scale contours represent, from black to white, $B_{\rm los} \leq -6$ G, $-6$ G $< B_{\rm los} \leq -2$ G, $-2$ G $< B_{\rm los} < 2$ G, 2 G $\leq B_{\rm los} < 6$ G, and $B_{\rm los} \geq 6$ G. In the two bottom panels, gray-scale contours represent, from black to white, $B_{\rm los} \leq -24$ G, $-24$ G $< B_{\rm los} \leq -8$ G, $-8$ G $< B_{\rm los} < 8$ G, 8 G $\leq B_{\rm los} < 24$ G, and $B_{\rm los} \geq 24$ G.

chunks of positive- and negative-polarity flux are found in proximity. Thus, even though the lower left quadrant of the λ8542 image is densely covered with strong positive-polarity flux elements, the coronal hole shows relatively little Fe IX or He II emission there; the bright plume in the middle of this dark region occurs near a large negative-polarity flux element.

Figure 3 (Plate L6) shows the north polar hole on 1996 November 8. Again, the compact fragments of positive- and negative-polarity flux in the photospheric λ8688 magnetogram appear to expand or coalesce into larger "jigsaw pieces" (mainly in the dominant polarity) in the chromospheric λ8542 magnetogram, while the relative amount of minority-polarity flux decreases.

Although the λ8542 magnetograms show the fields near the limb with remarkable clarity, we should bear in mind that this clarity comes at the sacrifice of the small-scale magnetic structure present at lower heights. Thus, referring to the area just inside the limb near the left edge of the images in Figure 3, we notice that strong Fe IX emission and bright He II network occur where no negative-polarity flux appears in the λ8542 magnetogram (although a very small amount of such flux is visible in higher-resolution versions of this magnetogram). By contrast, the λ8688 magnetogram clearly shows mixed-polarity flux in this region. (A similar "discrepancy" in which negative-polarity flux seems to be missing from the λ8542 magnetogram may be seen just inside the limb toward the right edge of these images.) Thus the photospheric magnetograms may reveal structure that is not present in the chromospheric magnetograms but that is nevertheless reflected in the EUV observations.

Figure 4 focuses on a particular area within the north polar hole on November 8 (the area appears to the left of center in the panels of Fig. 3). The Fe IX λ171 image (*top left*) shows a bright plume with a looplike structure along its northeast flank. From the λ8542 magnetogram (*middle left*) or its λ8688 counterpart (*middle right*), we see that the diffuse plume emission is centered on a region of negative-polarity flux located at the junction between two large chunks of positive-polarity flux, while the Fe IX loop forms a bridge between the negative-polarity region and the chunk of positive-polarity flux to its northeast. The locations of Fe IX emission closely match the He II λ304 network pattern (*top right*); thus, the bright plume occurs above an area of strongly enhanced network, while the position of the Fe IX loop coincides with that of an intense He II bright point.

The magnetograms displayed in the bottom panels of Figure 4 are the same as those in the middle panels, except that line-of-sight field strengths below 8 G have now been suppressed by readjusting the gray-scale contour levels. From the fact that the remaining flux is almost entirely of the majority (positive) polarity, we conclude that the minority-polarity fields associated with the plume emission and the helium enhancements are relatively weak ($|B_{\rm los}| \lesssim 8$ G). Indeed, it may be seen that the brighter EUV features are somewhat displaced from the centers of the strong unipolar flux concentrations.

Figure 5 (Plate L7) shows the south polar hole on 1996 December 1. As is evident from the λ8542 magnetogram, the south polar field is very strong and overwhelmingly negative in polarity. Although much of the polar hole area inside the limb is dark in Fe IX λ171, a bright plume appears where a strong positive-polarity flux element is sandwiched between large chunks of negative-polarity flux. The locations of diffuse Fe IX emission within the polar hole correspond well to the patterns of brightened He II λ304 network.

As a final example, Figure 6 (Plate L8) shows the north polar hole on 1996 August 14. Here, in addition to the λ8542 magnetogram and the Fe IX λ171 and He II λ304 EIT images, we display the He I λ10830 spectroheliogram taken at NSO/Kitt Peak. As expected (compare Harvey & Sheeley 1977), the network patterns traced out in emission by He II λ304 and in absorption by He I λ10830 are quite similar to each other inside the limb, and both roughly map out the areas of plume haze in Fe IX. The unusually bright plume structure near the left edge of the Fe IX image occurs where a large fragment of positive-polarity flux is in contact with negative-polarity flux; this region also coincides with strongly enhanced network in both helium lines. (By analogy with the example shown in Fig. 4, we would expect the intense core of this plume to contain one or more closed Fe IX loops.) The same bipole configuration, accompanied by intense helium network and strong (but perceptibly fading) plume emission, can also be seen 24 hr later in Figure 1.

## 4. SUMMARY AND DISCUSSION

This Letter has focused attention on magnetograms taken in Ca II λ8542 as a new tool in the study of the Sun's polar regions and of the polar coronal holes. These chromospheric magnetograms, now obtained regularly at NSO/Kitt Peak, show the strong polar fields near sunspot minimum with unprecedented clarity. We have visually compared a large number of these magnetograms taken between 1996 July and 1997 April (a few examples of which were displayed in § 3) with EIT images of

Fe IX λ171 plumes and He II λ304 network within the polar holes. Our conclusions may be summarized as follows:

1. Polar plumes occur where minority-polarity flux comes in contact with flux of the dominant polarity inside the polar coronal holes.
2. The base locations of diffuse Fe IX plume emission coincide roughly with the patterns of He II network brightenings within the coronal hole.
3. When a bright plume is seen inside the polar limb, the λ8542 magnetogram usually shows large, contiguous chunks of positive- and negative-polarity flux at the base of the plume, while the He II image shows strong, localized network emission.
4. In cases where the λ8542 magnetogram does not show clear evidence for minority-polarity flux at the base of a Fe IX plume, a He II bright point or localized network brightening is nevertheless usually found there, which suggests that one or more magnetic bipoles are indeed present (see Harvey 1985). The apparent absence of minority-polarity flux in the λ8542 magnetogram may be the result of time differences in the observations or insufficient sensitivity or spatial resolution. In some cases, minority-polarity flux may appear only in the "photospheric" λ8688 magnetogram, indicating the presence of bipolar flux that closes down at low heights.
5. Not every He II bright point or strong network enhancement shows significant Fe IX emission in its vicinity.
6. The darkest parts of the polar coronal hole in Fe IX λ171 and He II λ304 generally coincide with areas of the λ8542 magnetogram where little flux of either polarity is present or where flux of the dominant polarity occurs in isolation.

Observed with ~5″ spatial resolution (as here), the polar coronal holes near sunspot minimum are overwhelmingly unipolar, with the minority-polarity fields being weak compared with the majority-polarity component (see also Zhang, Zirin, & Marquette 1997). Thus, the imposition of a cutoff below $|B_{los}| \sim 20$ G on the line-of-sight polar fields (as in DeForest et al. 1997) would cause most of the minority flux to disappear from the magnetograms displayed in Figures 1–6. The brighter EIT plumes would then appear to be rooted next to (but not centered on) some of the remaining strong, isolated fragments of unipolar flux, as indicated in Figure 4 and as also found by DeForest et al. (1997) using *SOHO* MDI magnetograph observations of the south polar hole on 1996 March 7. The mixed-polarity nature of the flux underlying the polar plumes becomes apparent only when the threshold for $|B_{los}|$ is lowered to ~5–10 G. By implication, most of the open, unipolar flux emanating from the polar holes does not carry plume material, so polar plumes are not the main source of the high-speed polar wind. This conclusion is consistent with hydrodynamical energy-balance models for the plume and interplume regions of the polar coronal hole (Wang 1994).

Newkirk & Harvey (1968) were the first to suggest, based in part on a statistical correlation between the width of white-light polar plumes and the spacing between bright Ca II K3 network elements, that plumes are associated with unipolar flux concentrations inside the polar caps (see also Harvey 1965; Saito 1965; Suess 1982). However, they also noted that the number of such flux concentrations far exceeded the number of plumes. The current study indicates that it is the presence of minority flux (in the form of bipoles) that "activates" a given flux concentration so that it becomes the site of a plume.

Our conclusions are consistent with those of an earlier investigation employing *Skylab*-era data (Wang & Sheeley 1995). There, a mechanism for plume formation was proposed whereby bipoles interact with unipolar flux concentrations at the supergranular boundaries. In this exchange of open and closed magnetic flux, the minority-polarity end of each bipole reconnects with a unipolar flux element, forming a new closed loop, while the opposite end of the bipole opens up, releasing its trapped energy in the form of a plume. The plume thus represents open magnetic field of the dominant polarity, but its existence requires the presence of one or more bipoles as well as a unipolar flux concentration (by themselves, neither bipoles nor unipolar flux elements would give rise to plumes, although isolated bipoles would still produce enhanced EUV network emission and bright points). This and other possible mechanisms might be tested by means of coordinated, higher cadence EIT and Ca II λ8542 observations of large, bright plumes rooted inside the polar limb.

This study was made possible only through the efforts of the entire *SOHO* EIT team. The NSO/Kitt Peak data used here were produced cooperatively by NSF/NOAO, NASA/GSFC, and NOAA/SEC.

## REFERENCES

Ahmad, I. A., & Withbroe, G. L. 1977, Sol. Phys., 53, 397
Bohlin, J. D., Sheeley, N. R., Jr., & Tousey, R. 1975, in Space Research XV, ed. M. J. Rycroft (Berlin: Akademie), 651
Chapman, G. A., & Sheeley, N. R., Jr. 1968a, Sol. Phys., 5, 442
———. 1968b, in IAU Symp. 35, Structure and Development of Solar Active Regions, ed. K. O. Kiepenheuer (Dordrecht: Reidel), 161
DeForest, C. E. 1995, Ph.D. thesis, Stanford Univ.
DeForest, C. E., et al. 1997, Sol. Phys., submitted
Delaboudinière, J.-P., et al. 1995, Sol. Phys., 162, 291
Giovanelli, R. G. 1980, Sol. Phys., 68, 49
Habbal, S. R. 1992, Ann. Geophys., 10, 34
Habbal, S. R., Esser, R., Guhathakurta, M., & Fisher, R. R. 1995, Geophys. Res. Lett., 22, 1465
Harvey, J. W. 1965, ApJ, 141, 832
Harvey, J. W., & Sheeley, N. R., Jr. 1977, Sol. Phys., 54, 343
Harvey, K. L. 1985, Australian J. Phys., 38, 875
Jones, H. P. 1985, Australian J. Phys., 38, 919
Jones, H. P., Duvall, T. L., Jr., Harvey, J. W., Mahaffey, C. T., Schwitters, J. D., & Simmons, J. E. 1992, Sol. Phys., 139, 211
Livingston, W. C., Harvey, J., Pierce, A. K., Schrage, D., Gillespie, B., Simmons, J., & Slaughter, C. 1976a, Appl. Opt., 15, 33
Livingston, W. C., Harvey, J., Slaughter, C., & Trumbo, D. 1976b, Appl. Opt., 15, 40
Newkirk, G., Jr., & Harvey, J. 1968, Sol. Phys., 3, 321
Pope, T., & Mosher, J. 1975, Sol. Phys., 44, 3
Saito, K. 1965, PASJ, 17, 1
Suess, S. T. 1982, Sol. Phys., 75, 145
Wang, Y.-M. 1994, ApJ, 435, L153
Wang, Y.-M., & Sheeley, N. R., Jr. 1995, ApJ, 452, 457
Widing, K. G., & Feldman, U. 1992, ApJ, 392, 715
Zhang, L. D., Zirin, H., & Marquette, W. H. 1997, Sol. Phys., in press

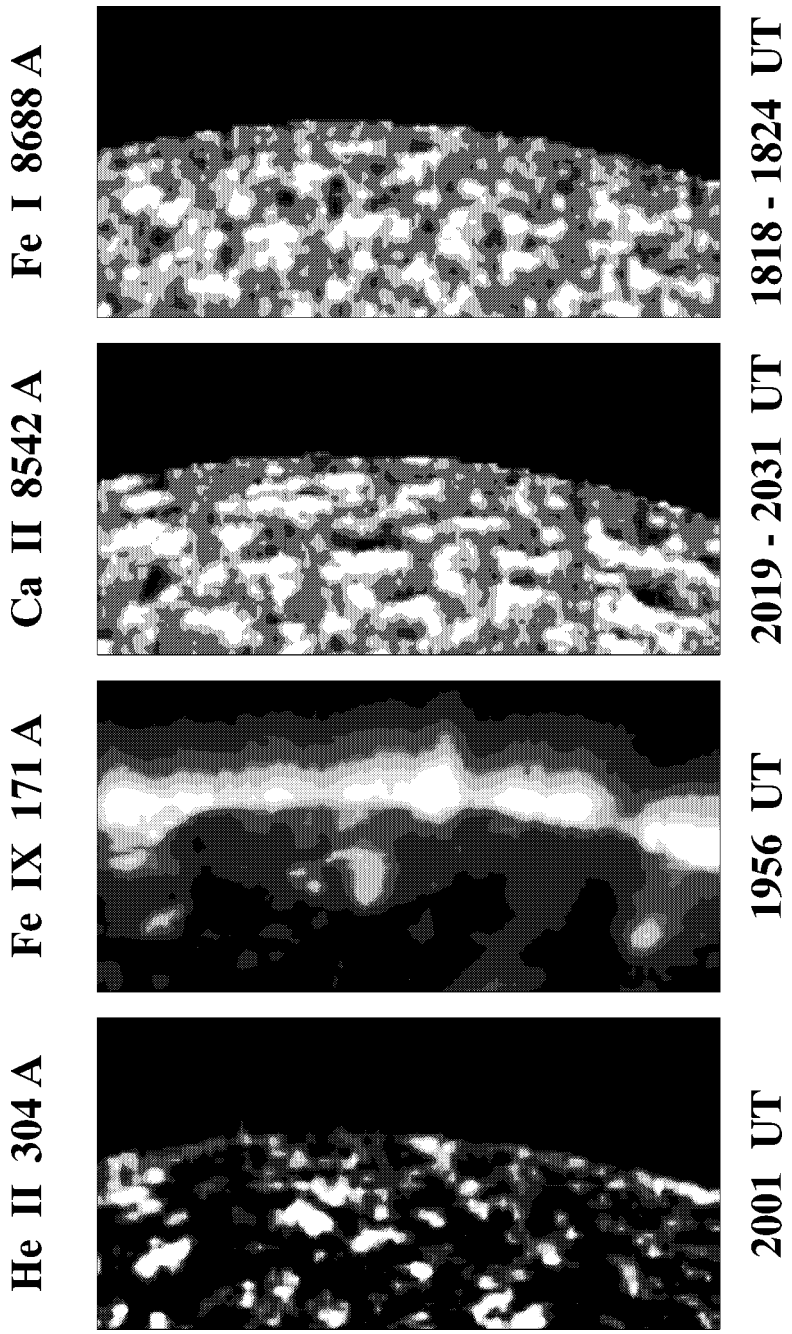


FIG. 1.—North polar hole on 1996 August 15. Times of observation are given to the right of each panel. The four images are in approximate register and show the same portion of the solar disk. *Top panel*: NSO magnetogram in the "photospheric" line Fe I λ8688. Gray-scale contours indicate the strength and polarity of the line-of-sight field component: the five shades represent, from black to white, $B_{los} \leq -6$ G, $-6$ G $< B_{los} \leq -2$ G, $-2$ G $< B_{los} < 2$ G, 2 G $\leq B_{los} < 6$ G, and $B_{los} \geq 6$ G. *Second panel*: NSO magnetogram in the chromospheric line Ca II λ8542 (gray-scale contours as in the λ8688 magnetogram). *Third panel:* EIT spectroheliogram in the Fe IX λ171 emission line, showing polar plumes rooted at and inside the limb. *Bottom panel:* EIT spectroheliogram in the He II λ304 emission line, showing areas of brightened network inside the otherwise dark polar coronal hole.

WANG et al. (see 484, L76)

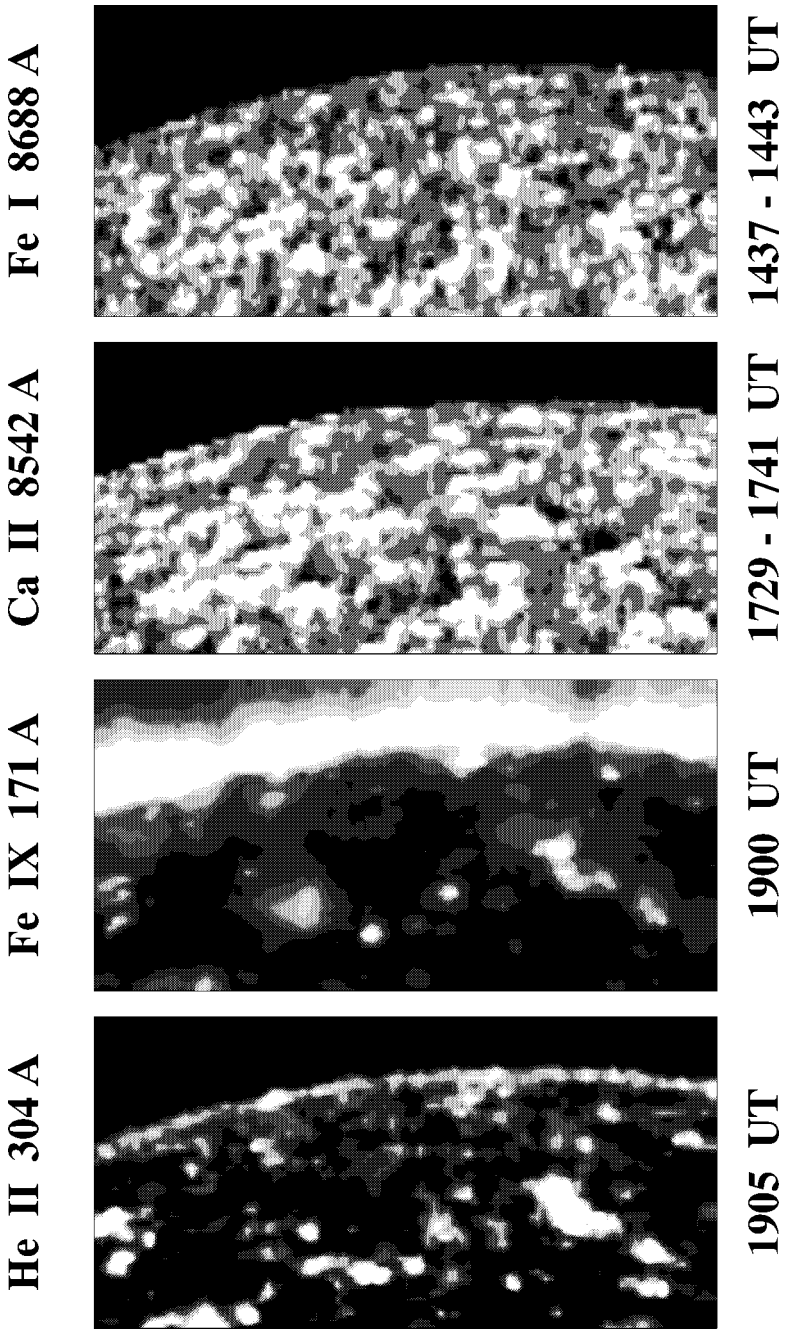


FIG. 2.—North polar hole on 1996 October 12 (for key, see Fig. 1 legend).

WANG et al. (see 484, L76)

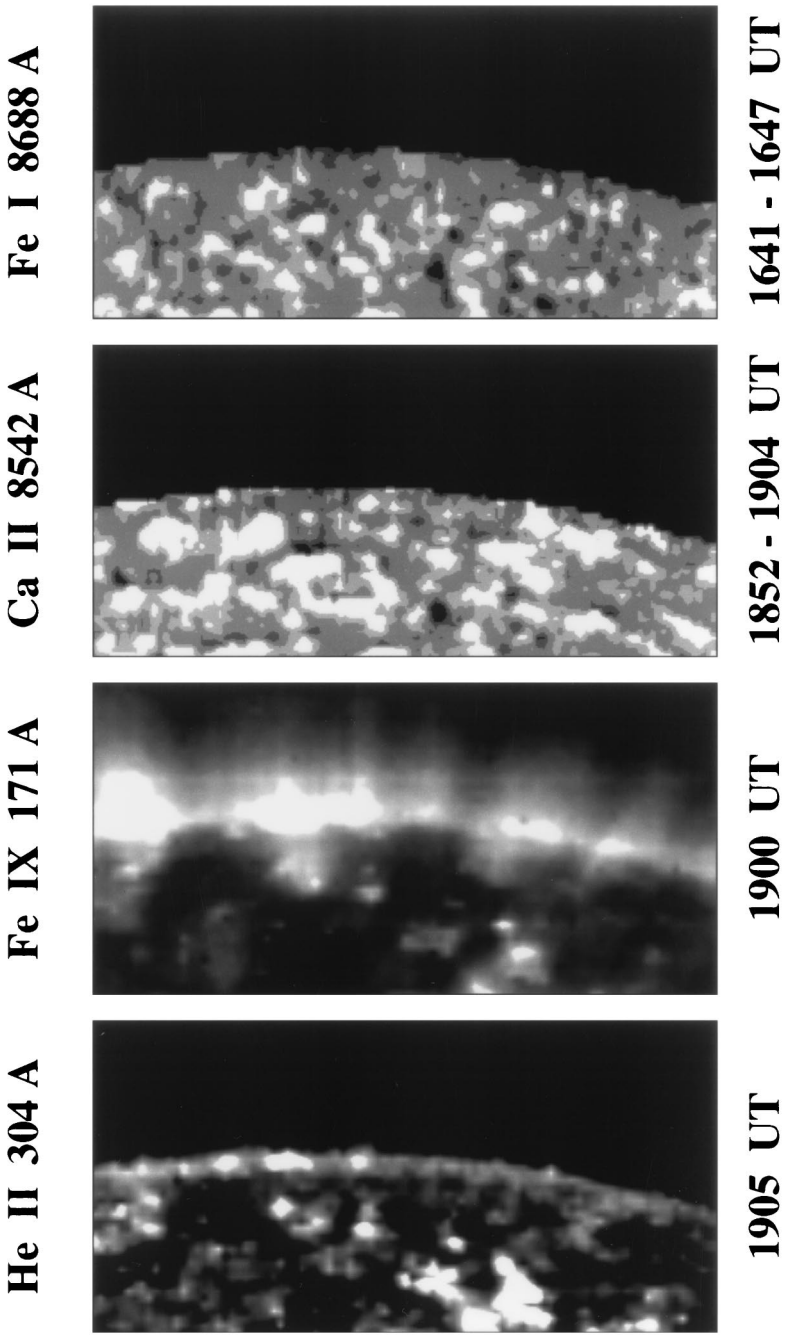


FIG. 3.—North polar hole on 1996 November 8 (for key, see Fig. 1 legend).

WANG et al. (see 484, L77)

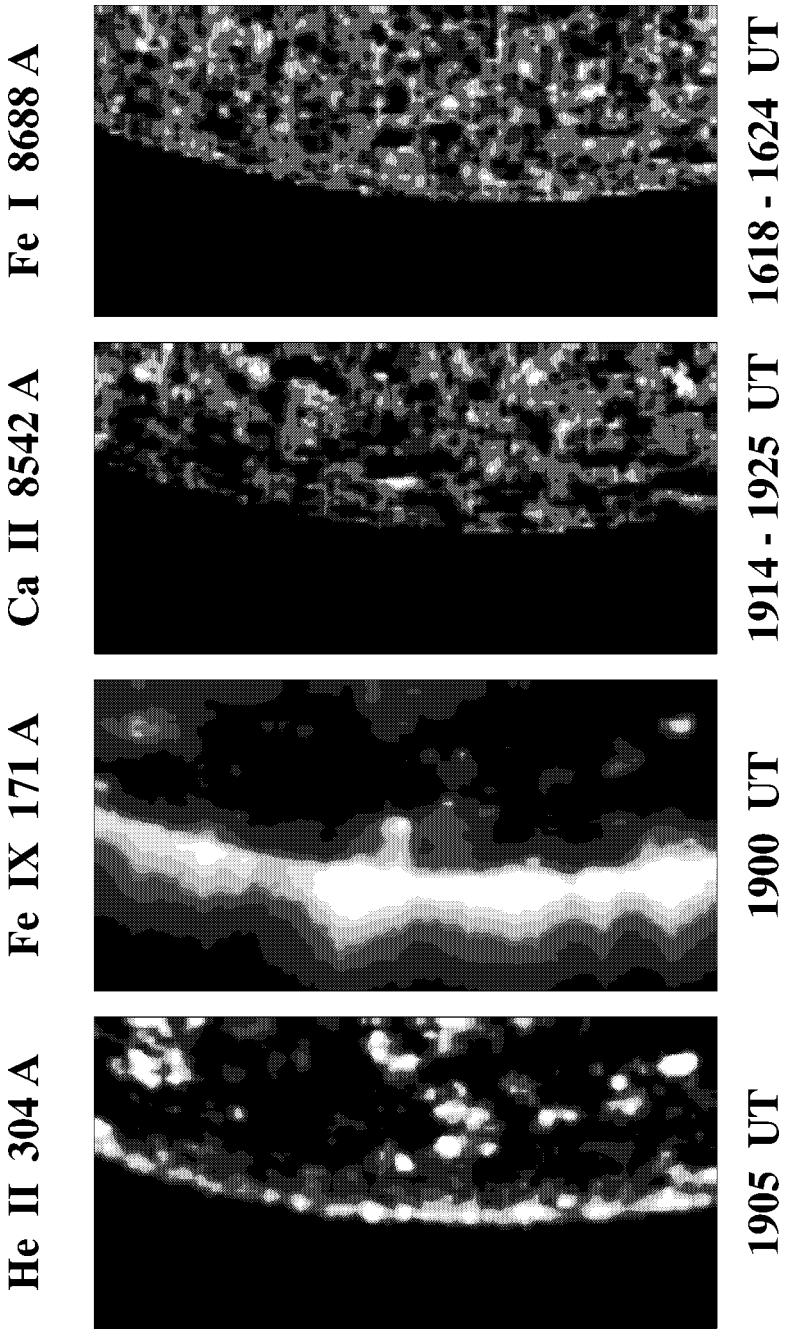


FIG. 5.—South polar hole on 1996 December 1 (for key, see Fig. 1 legend).

WANG et al. (see 484, L77)

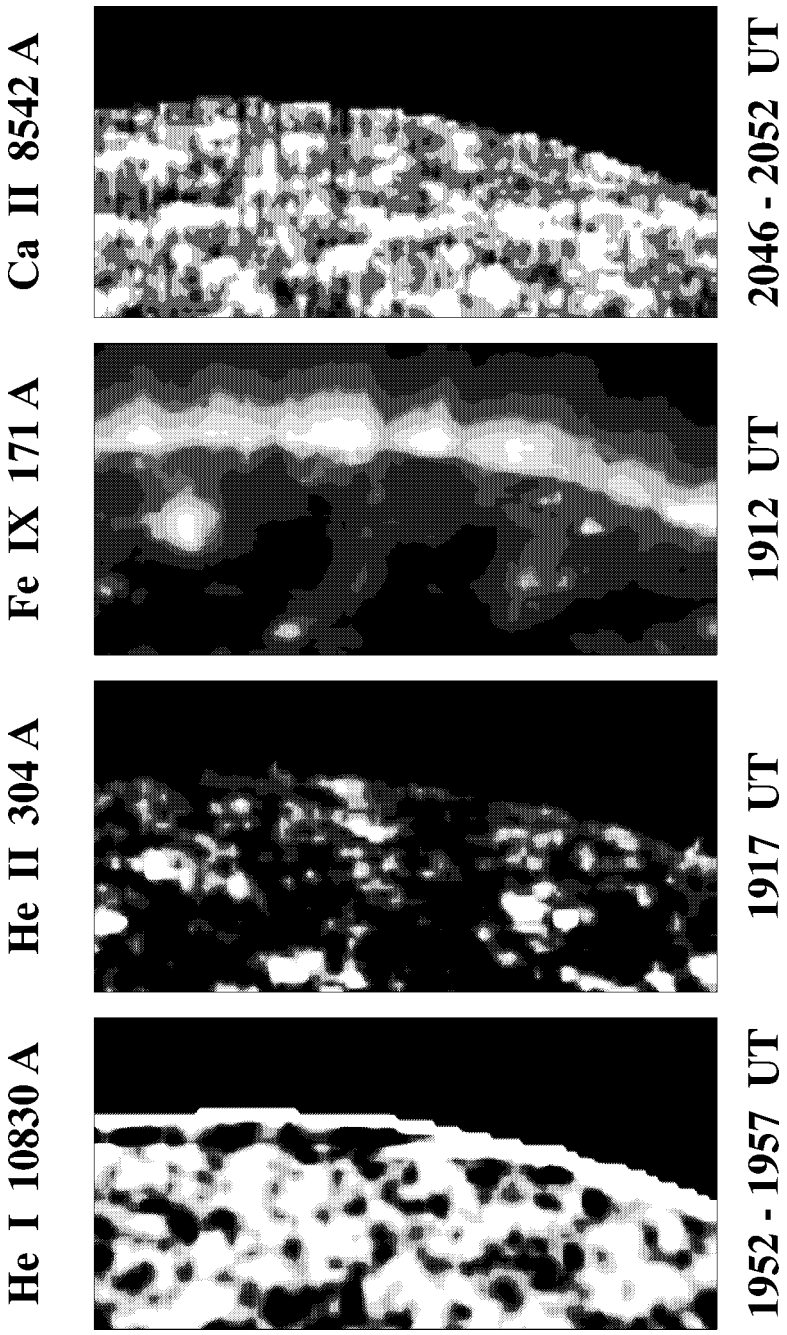


FIG. 6.—North polar hole on 1996 August 14. *Top panel*: NSO magnetogram in Ca II λ8542 (gray-scale levels as in Fig. 1). *Second panel:* EIT spectroheliogram in the Fe IX λ171 emission line. *Third panel:* EIT spectroheliogram in the He II λ304 emission line. *Bottom panel:* NSO spectroheliogram in the He I λ10830 absorption line.

WANG et al. (see 484, L77)